Unraveling the mesoscale functional connectivity of the human primary visual cortex using high-resolution functional MRI

Marianna E. Schmidt[1,2+], Iman Aganj[3,4+], Jason Stockmann[3,4], Berkin Bilgic[3-5], Yulin Chang[6], W. Scott Hoge[7], Evgeniya Kirilina[1], Nikolaus Weiskopf[1,8,9], & Shahin Nasr[3,4*]

Affiliations:

[1] Department of Neurophysics, Max Planck Institute for Human Cognitive and Brain Sciences, Leipzig, Germany

[2] Max Planck School of Cognition, Leipzig, Germany

[3] Athinoula A. Martinos Center for Biomedical Imaging, Massachusetts General Hospital, Boston, MA, USA

[4] Radiology Department, Harvard Medical School, Boston, MA, USA

[5] Harvard/MIT Health Sciences and Technology, Cambridge, MA, United States

[6] Siemens Medical Solutions USA Inc., Malvern, PA, USA

[7] Imaginostics, Inc., Orlando, FL, USA

[8] Felix Bloch Institute for Solid State Physics, Faculty of Physics and Earth System Sciences, Leipzig University, Leipzig, Germany

[9] Wellcome Center for Human Neuroimaging, Institute of Neurology, University College London, London, UK

[+] **Co-first authors**

* **Corresponding author:** Shahin Nasr, Ph. D.

Email address: shahin.nasr@mgh.harvard.edu

Abstract

Despite their importance in shaping visual perception, functional connectivity between ocular dominance columns (ODCs), the building blocks of neuronal processing within the human primary visual cortex (V1), remains largely unknown. Using high-resolution functional MRI (fMRI), we localized ODCs and assessed their resting-state functional connectivity (rs-FC) in 11 human adults (3 females). Consistent with anatomical studies in animals, we found stronger rs-FC in the middle compared to deep and superficial cortical depths and selectively stronger rs-FC between ODCs with alike compared to unalike ocular polarity. Beyond what was known from animal models, and consistent with human perceptual biases, we found stronger intra- and interhemispheric rs-FC in peripheral (compared to central) and in dorsal (compared to ventral) V1 subregions. Lastly, we found a significant correlation between rs-FC patterns and ODC maps, supporting the hypothesis that ODC maps can be predicted from rs-FC patterns within V1. These results highlight the heterogeneity in functional connectivity between ODCs across cortical depths and V1 subfields, underscoring their likely association with human perceptual biases.

Keywords: ODCs, resting-state fMRI, mesoscale functional organization, cortical heterogeneity, human visual cortex

Significance Statement

- Our findings provide evidence for selective mesoscale rs-FC between ODCs, aligning with prior anatomical findings in animals.
- Beyond what is known from animal studies, we demonstrate that the mesoscale rs-FC pattern varies across V1 subregions, aligning with the expected heterogeneity in global visual processing across visual subfields.
- We provide evidence for the predictability of ODC maps from the rs-FC pattern, establishing one of the first steps toward leveraging rs-FC for segmentation of the visual cortex at mesoscale levels.

Abbreviations

ODCs: Ocular Dominance Columns

FMRI: Functional Magnetic Resonance Imaging

RS-FC: Resting-state Functional Connectivity

DE: Dominant Eye

NDE: Non-Dominant Eye

ODI: Ocular Dominance Index

ROI: Region Of Interest

RM-ANOVA: Repeated Measures Analysis of Variance

1. Introduction

In humans and many animals, the visual cortex is organized into neuronal columns that encode visual features. Despite their central role in shaping perception, the functional connectivity between cortical columns in the human visual cortex remains poorly understood. This gap in our knowledge stems primarily from the limited spatial resolution of conventional neuroimaging techniques relative to the size of cortical columns and layers. As a result, much of our understanding of the mesoscale organization of the visual cortex relies on anatomical studies in animals using invasive techniques that are not applicable to humans in vivo. To bridge this knowledge gap, we leveraged high-resolution functional MRI (fMRI) to investigate resting-state functional connectivity (rs-FC) between ocular dominance columns (ODCs), which are considered the building blocks of visual processing in the primary visual cortex (V1).

Anatomical studies in non-human primates (NHPs) have revealed that ODCs as far as 8 mm apart are systematically interconnected via horizontal fibers [1–6]. These fibers are most dense in the middle cortical layers, particularly layer 4B, preferentially connecting ODCs with alike rather than unalike ocular polarity. The level of this bias in the number of horizontal fibers remains a matter of debate varying from 4% [4] to 15% [7] in favor of the ODC pairs with alike ocular polarity. However, the reason for this inconsistency could not be tested systematically due to the limited samples.

Functional evidence for the biased structural connectivity between alike ODCs is provided by electrophysiological [8–10] and optical imaging studies [11]. According to these studies, neurons with alike rather than unalike ocular polarity exhibit stronger synchronized activity. Interestingly, this synchronous activity is detectable over distances up to 20 mm [11] indicating that the selective functional connectivity between ODCs extends far beyond the range of monosynaptic horizontal fibers and cannot be attributed to the overlapping receptive field sizes of the targeted neurons [10].

Evidence for homologous functional organization within human V1 is currently nonexistent. This is mainly due to difficulties in studying ODCs based on conventional neuroimaging techniques that provide a low signal-to-noise ratio and poor spatial resolution (>2mm), inadequate for studying the mesoscale functional organization of the human visual cortex. Nonetheless, at coarser levels, fMRI studies have shown higher intra- and interhemispheric rs-FC between V1 subregions representing similar locations of the visual field [12,13]. Outside V1, high-resolution fMRI has successfully been used to study rs-FC between color-, stereo- as well as motion-selective cortical columns across extrastriate visual areas [14–17]. Findings from these studies have supported the hypothesis that cortical columns with alike stimulus preferences are more selectively connected to each other, and that this selectivity can be detected by high-resolution resting-state fMRI (see also [18]).

Using high-resolution fMRI in the past, multiple groups have successfully localized ODCs in humans [14,19–22]. In this study, we extended the application of high-resolution fMRI to study the rs-FC between ODCs, in the absence of any visual input (eyes closed), in 11 adult humans. We examined the influence of cortical depth, pairwise distance, relative ocular polarity (i.e., alike vs. unalike ocular preference), and ocular preference level on the mesoscale rs-FC within V1 and assessed the heterogeneity of the measurements across V1 subregions. These analyses were then extended to evaluate the mesoscale rs-FC between V1 subregions within and across the two hemispheres. Lastly, we tested the predictability of ODC maps based on the mesoscale rs-FC pattern within V1. Our findings provide new insights into the mesoscale functional organization of V1, offering insights beyond what was previously known from animal studies. A preliminary version of some of the results has been presented at a workshop [23].

2. Methods

2.1. Participants

11 subjects (3 females), aged 25-45 years, participated in this study. All participants had radiologically intact brains, intact vision, and no history of neuropsychological disorders. All experimental procedures conformed to the guidelines of the National Institutes of Health (NIH) and were approved by the Mass General Brigham Institutional Review Board. Written informed consent was obtained from all participants prior to all experiments.

2.2. Procedure

Each participant was scanned in an ultra-high-field (7T) MRI scanner to collect resting-state data. To test the reproducibility of the findings, four of the participants—selected based on availability—were rescanned on a different day using a different 7T scanner to recollect resting-state data. For each participant, ODC and retinotopic maps were obtained from a separate set of scans [21]. Structural scans were acquired on a 3T scanner.

2.2.1. Resting-state measurements

To collect spontaneous fMRI activity, each participant was scanned for 3 to 4 runs (512 s per run), except for one individual who was scanned for just one run due to time limitations. Participants were instructed

to keep their eyes closed for the duration of the run but not to fall asleep. We communicated with participants between runs to ensure they remained awake during the scan.

2.2.2. ODC mapping

ODC mapping was conducted on different days from the resting-state session. Details of the procedure are already described comprehensively in our recent publication [21]. Briefly, the ODC map was determined by contrasting the fMRI activity evoked in response to stimulation of the dominant eye (DE) vs. non-dominant eye (NDE) in a block design. The stimuli consisted of sparse (5%) horizontally moving random dots (-0.22° to 0.22°; 0.3 Hz), with red (50% of blocks) and green (remaining blocks) dots (0.09° × 0.09°; 56 cd/m²), presented against a black background. Participants viewed the stimuli through custom-made anaglyph spectacles (with red and green filters) mounted on the head coil. The stimuli spanned 20° × 26° in the visual field. Filter laterality (i.e., red-left vs. red-right) was counterbalanced between sessions and across participants.

2.2.3. Retinotopic mapping

The borders of retinotopic visual areas were defined by mapping the horizontal vs. vertical meridians [24,25]. Stimuli consisted of flashing radial checkerboards within retinotopically defined wedge-shaped apertures, extending radially along either the horizontal or vertical meridians (polar angle = 30°) and presented against a gray background. Further details are provided in our previous publication [21].

2.3. Imaging

2.3.1. Main experiments

For the resting-state fMRI measurements, and ODC and retinotopic mapping, we utilized a 7T whole-body Siemens scanner equipped with SC72 body gradients (70 mT/m gradient strength and max slew rate of 200 T/m/s), a custom-built 32-channel helmet radio-frequency (RF) receive coil array, and a birdcage volume RF transmit coil. Resting-state data were collected using single-shot 2D gradient-echo EPI, with 1.0 mm isotropic nominal voxel size, with the following protocol parameter values: TR=4000 ms, TE=28 ms, excitation flip angle=85°, field of view (FOV) matrix=192×192, BW=1184 Hz/pixel, echo-spacing=1 ms, 7/8 phase partial Fourier, 59 oblique-coronal slices covering occipital lobe, acceleration factor R=4 with GRAPPA reconstruction and FLEET-ACS data (Polimeni et al., 2015) with a 10° flip angle. For

ODC and retinotopic mapping, we used a similar EPI protocol with TR=3000ms, flip angle=78°, and 44 oblique-coronal slices.

2.3.2. Reproducibility tests

To test the reproducibility of the resting-state results, 4 participants were scanned again (on a different day) in a Siemens MAGNETOM Terra whole-body MRI (80 mT/m gradient strength and max slew rate of 200 T/m/s). In contrast to the other 7T scanner (see above), this scanner provides passive and active shimming up to 3rd order and is equipped with an in-house-built head RF coil systems that use a quadrature birdcage transmit coil along with a close-fitting 64-ch RF receive array [26]. In these sessions, we used single-shot 2D gradient-echo EPI, with 1.0 mm isotropic voxel size, with the following protocol parameter values: TR=4000 ms, TE=25 ms, flip angle=80°, FOV matrix=180×180, BW=1158 Hz/Px, echo-spacing=1 ms, 7/8 phase partial Fourier, 66 oblique-coronal slices covering occipital cortex, and FLEET-ACS data [27] with 10° flip angle. We also used R=4 dual-polarity GRAPPA reconstruction for improved Nyquist ghost correction [28].

2.3.3. Structural scans

At ultra-high field (7T), T1-weighted anatomical brain images typically suffer from image contrast variations (bias field) over the FOV due to the combined effects of: (a) transmit RF field inhomogeneity caused by dielectric wavelength effects within the head [29] and (b) disrupted inversion pulses in areas where tissue susceptibility interfaces perturb the static magnetic field [30]. To avoid this issue, we used anatomical images acquired at 3T on a Siemens TimTrio whole-body scanner, equipped with the standard vendor-supplied 32-channel RF head coil array, which provides relatively uniform image contrast over the full FOV. We used a 3D T1-weighted MPRAGE sequence with protocol parameter values: TR=2530 ms, TE=3.39 ms, TI=1100 ms, flip angle=7°, bandwidth=200 Hz/pix, echo spacing=8.2 ms, voxel size=1.0×1.0×1.0 mm^3, and FOV=256×256×170 mm^3.

2.4. Data analysis

Functional and anatomical MRI data were pre-processed and analyzed using FreeSurfer (version 7.4.0; http://surfer.nmr.mgh.harvard.edu) [31] and in-house MATLAB and Python code.

183 **2.4.1. Anatomical data**

184 **2.4.1.1. Defining cortical surfaces**

185 The anatomical data of each participant was used to reconstruct individual inflated and flattened cortical
186 surfaces [32]. In this process, the standard pial surface was defined as the boundary between the gray matter
187 (GM) and the surrounding cerebrospinal fluid (CSF), while the white matter (WM) surface was generated
188 as the interface between the WM and GM. Additionally, nine intermediate surfaces were created, spaced
189 at intervals of 10% of the cortical thickness.

190

191 **2.4.1.2. Defining cortical depths**

192 To examine the impact of cortical depth on rs-FC, the GM was divided into deep, middle, and superficial
193 cortical depths (Figure 1A). The deep cortical depth was defined as the region between the WM-GM
194 interface and the two adjacent surfaces above it. The superficial cortical depth was defined as the region
195 between the GM-CSF interface and the two adjacent surfaces below it. The middle cortical depth included
196 the three intermediate reconstructed surfaces. Notably, this approach left one intermediate surface gap
197 between these depth levels to improve the separation of the three segments. To enhance the co-
198 registration of functional and structural scans, all surfaces were upsampled to a 0.5 mm resolution using
199 our previously introduced pipeline [33].

200

201 **2.4.2. Functional data**

202 **2.4.2.1. Preprocessing**

203 All functional data were preprocessed with a pipeline for high-precision ultra-high-resolution fMRI [33].
204 Briefly, the collected functional data were first upsampled to 0.5 mm isotropic resolution. For each
205 participant, functional data from each run were rigidly aligned (with 6 degrees of freedom) to their
206 structural scan using rigid Boundary-Based Registration [34]. Head motion covariates were then derived for
207 six directions. After motion correction, intensity normalization was applied to the fMRI data. For the
208 resting-state data, the preprocessing pipeline was slightly adjusted. Specifically, before upsampling to 0.5
209 mm, the data were denoised using the NORDIC approach [35] and slice timing corrected [31]. Additionally,
210 the data were detrended for quadratic trends and high-pass filtered using a cut-off frequency of 0.01 Hz [36].

211 To preserve spatial resolution on the surface, no tangential spatial smoothing was applied to the fMRI
212 data. Instead, radial (intracortical) smoothing—perpendicular to the cortex and within cortical columns—
213 was used [37]. For ODC and retinotopic mapping, to minimize the blurring impact of pial veins on

214 functional map resolution [14,38–40], radial smoothing was restricted to the deep cortical depth (as defined in
215 2.4.1.2). For rs-FC analysis, radial smoothing was applied either to the entire GM (sections 3.1-3.2) or
216 separately to the deep, middle, and superficial cortical depths (sections 3.3-3.6). Notably, previous studies
217 in NHPs [41] and humans [21] have shown that the ODC maps remain mostly unchanged across the cortical
218 depth levels.

219

220 **2.4.2.2. Resting-state functional data**

221 The rs-FC between pairs of vertices within the flattened cortical surface mesh of V1 was measured by
222 estimating Pearson's partial correlation coefficients of their resting-state fMRI time series. For this first
223 level statistical analysis, the estimated six head motion parameters as well as the mean WM signal were
224 included as nuisance regressors. Notably, the rs-FC analysis did not include correlations between vertex
225 pairs located at different cortical depths considering the organization of horizontal fibers (i.e., primarily
226 parallel to the cortical surface). For our downstream analyses, which required linear statistical operations
227 on correlation values, we used Fisher *z*-transformed correlation values that are expected to have a
228 distribution closer to normal than Pearson's correlation coefficients do and are thus more suitable for
229 parametric calculations.

230

231 **2.4.2.3. ODC and retinotopic mapping**

232 Details of the data analysis for mapping ODCs and retinotopic visual areas are described in our recent
233 publication [21]. Briefly, after preprocessing (see above), a standard hemodynamic response model based on
234 a gamma function was fitted to the signals from deep cortical depths to estimate the amplitude of the
235 blood-oxygen-level-dependent (BOLD) response. To generate differential maps of DE vs. NDE
236 activation, a vertex-wise general linear model was applied by computing the contrast of interest. The
237 resulting beta and significance maps were projected onto each participant's anatomical volumes and
238 reconstructed cortical surfaces (Figure 1B). The reproducibility of the maps across scan sessions was
239 tested and proved for all individual participants [14,21]. As noted above, only data from deep cortical depths
240 were used for ODC and retinotopic mapping.

241

242 **2.5. Statistical analysis**

243 As a second-order statistical analysis (see also Section 2.4.2.2), we assessed the significance of the impact
244 of the following independent parameters on rs-FC: (1) relative ocular polarity, (2) distance between

vertices, (3) level of ocular preference (ocular dominance index (ODI)), (4) cortical depth, and (5) region of interest (ROI). These parameters were calculated as follows.

2.5.1. Distance between vertex pairs

The distance between vertices in each pair was calculated as the Euclidean distance on the flattened cortical surface. To minimize the bias in the rs-FC resulting from the effect of the fMRI point spread function (PSF), we excluded vertex pairs located closely together (<3 mm) [42–44]. Since vertex pairs with alike ocular polarity (see below) generally were closer together than unalike pairs, we used random subsampling to balance the distance distributions between alike and unalike vertex pairs. To that end, we divided the distance distribution of all vertex pairs into 100 quantiles, for each of which, we then determined the counts of alike and unalike vertex pairs and randomly discarded excess pairs from the larger group to equalize their numbers. Because V1 varied in size across participants, vertex pairs for each participant were divided into 10 distance quantiles, with 1 referring to the shortest distances and 10 referring to the longest distance. The quantile rank (rather than the absolute distance) was used for further statistical analysis. The median distance for each quantile is shown in Figure S1. The distance between vertex pairs was then used as a numerical parameter in the statistical tests.

2.5.2. Relative ocular polarity of vertices

To assess the effect of relative ocular polarity on rs-FC, a pair of vertices was classified as alike or unalike when the ocular preferences of the two vertices were the same (i.e. both vertices responded preferentially to the same eye) or opposite, respectively. The relative ocular polarity was then used as a categorical parameter in the statistical tests. Notably, the ocular preference of each vertex was determined based on the unthresholded ODC map (Figure 1B). Consistent with our previous findings in a smaller group of participants [21], the number of vertices responding preferentially to DE and NDE stimulation, as well as the amplitude of ocular-preferring activity (i.e., the response to the preferring vs. non-preferring eye stimulation), did not differ significantly across participants (Figure S2). This result indicates that both eyes were represented equally within V1.

2.5.3. Ocular dominance index (ODI)

To assess the impact of ocular preference level on rs-FC, we used a method similar to the one introduced by Hubel and Wiesel (1982) and later adopted by others [45–48]. Specifically, for each vertex, the level of

ocular preference — i.e., the estimated beta value for differential response to preferred vs. non-preferred eye stimulation —was measured during ODC mapping. For each subject, these beta values were divided into 10 quantiles, with 1 representing the weakest ocular preference and 10 representing the strongest. The quantile rank (rather than the absolute ocular preference) was then used as the ODI. The median beta value for each ODI is shown in Figure S3.

The effect of ODI on rs-FC between vertex pairs was tested by grouping vertices into 5 cumulative categories: (1) vertex pairs from quantiles 1 and 2, (2) quantiles 1 to 4, (3) quantiles 1 to 6, (4) quantiles 1 to 8, and (5) quantiles 1 to 10.

2.5.4. Cortical depths

To test the impact of cortical depth on the level of rs-FC, the rs-FC data analysis was conducted separately for the deep, middle, and superficial depths of the GM. The cortical depth was then used as a categorical parameter in the statistical tests.

2.5.5. ROI

In the main analysis (sections 3.1 to 3.3), the ROI included the stimulated portion of V1 (radius<10°) except for a small dorsal region along the V1-V2 border (Figure 1C) where ODCs could not be identified due to occlusion of the ventral visual field by the nose [21]. To evaluate the heterogeneity of rs-FC within V1, we manually divided the stimulated part of V1 into equisized dorsal and ventral as well as central (radius<4°) and peripheral (4°<radius<10°) subregions and compared the rs-FC within these subdivisions (see sections 3.4 and 3.5). The ROI was then used as a categorical parameter in the statistical tests.

2.5.6. Statistical tests

2.5.6.1. Repeated measures (RM) ANOVA

RM-ANOVA was primarily used to test the impact of independent parameters (see above) on the measured rs-FC between the vertex pairs. Specifically, we first tested the impact of relative ocular polarity (alike vs. unalike) and distance using a two-way RM-ANOVA (Section 3.1). Second, for a subset of 4 participants, the reproducibility of the results was tested by adding the session number (categorical: 1st vs. 2nd) to the independent parameters (i.e., distance and relative ocular polarity) and applying a three-way RM-ANOVA (Section 3.2).

The impact of ODI (5 cumulative categories, see Section 2.5.3) and cortical depth, along with relative ocular polarity, was tested by applying a three-way RM-ANOVA (Section 3.3). Lastly, heterogeneity of intrahemispheric and interhemispheric rs-FC measurements was tested by including V1 subregions (ROIs) in the list of independent parameters and applying a four-way RM-ANOVA (sections 3.3 and 3.4).

Notably, in all tests except for interhemispheric rs-FC measurements, the rs-FC values from the two hemispheres were averaged to improve the signal-to-noise ratio. Considering that RM-ANOVA is particularly susceptible to violations of the sphericity assumption, caused by the correlation between measured values and unequal variance of differences between experimental conditions, results were corrected, when necessary (as determined using a Mauchly test), using the Greenhouse-Geisser method. A p-value of <0.05 was considered statistically significant.

2.5.6.2. Linear mixed effects (LME) model

To ensure that overlap between the cumulative ODI categories did not skew the estimated significance of our results, we conducted a supplementary analysis based on using an LME model to assess the relationship between rs-FC and relative ocular polarity, ODI, and cortical depth accounting for subject-level variability (random intercepts by subject). In this analysis, rather than using the cumulative ODI categories, we used the product of BQ_1 and BQ_2 (i.e. BQ_{12}), where BQ_1 and BQ_2 represent the ODIs of the first and second vertices in a pair. Since this created a symmetric matrix of 10×10 categories, we excluded the redundant upper triangle, resulting in 55 joint ODI categories, which were then used in an LME model (see Section 2.5.6.2). By using 55 non-overlapping joint ODI brackets, we ensured that the significance of the results was not overestimated due to datapoint (vertex pair) interdependencies.

To apply the model the MATLAB command `fitlme` was used according to the following formula:

$$rsFC \sim BQ_{12} + CD + ROP + BQ_{12} * CD + BQ_{12} * ROP + CD * ROP + BQ_{12} * CD * ROP + (1|Subject),$$

where BQ_{12} represents the product of the ODIs of the first and second vertices in a pair, CD represents cortical depth, and ROP is relative ocular polarity. This approach enabled us to check for the consistency of the results obtained by ANOVA and LME. Notably, in contrast to ANOVA, LME takes the hierarchical structure of the data into account. This method further allowed us to quantify the independent contributions of the main factors and their interactions while controlling for variability across subjects (see Section 3.3). A p-value of <0.05 was considered statistically significant.

2.5.6. Correlation between rs-FC and ODC maps

To evaluate how well rs-FC reflects the underlying ODC map, we conducted a correlation analysis. We selected 1000 seed vertices at random within V1 (far enough from the V1 border) and correlated each seed vertex's resting-state fMRI time-series with the rest of the vertices in a 2D donut-shaped region (ring) centered at that seed vertex, generating 1000 2D rs-FC maps. To investigate the impact of distance, we conducted the analysis multiple times within concentric rings around each seed vertex with varying outer radius ranging from 4 to 10 mm. Similarly to our main analyses, we excluded nearby target vertices falling within an inner radius of 3 mm to minimize potential biases caused by the PSF of the BOLD signal [42–44]. Within each ring, we calculated the correlation between the rs-FC map and the underlying ODC map, which constitutes the correlation value under the alternative hypothesis (H1) that rs-FC and ODC maps are related. For each ring size, the resultant correlation values were averaged across the 1000 sampled sites.

To determine the statistical significance of our results, we compared these correlations to null-hypothesis (H0) distributions (correlations between unrelated rs-FC and ODC maps) generated by correlating the rs-FC values in each ring with the ODC differential map in a spatially shifted (misaligned) ring ($H0_a$) as well as a 180° rotated ring ($H0_b$). With this approach, we tested whether the observed correlations were meaningful and not solely due to the inherent spatial structure of the ODC map. To ensure that interpolation and resampling artifacts affected both the null and alternative tests similarly, in all experiments, we resampled the rs-FC and ODC map values with nearest-neighbor interpolation on a set of points generated via 2D quasi-random Halton sampling [49,50] and distributed with a density of 10 points per mm^2.

2.6. Data availability statement

The data and code will be shared upon reasonable request.

3. Results

Studies in NHPs suggest that horizontal fibers are more numerous in the middle layer (layer 4B) compared to deeper (layers 5 and 6) and superficial cortical layers (layers 2 and 3). They also indicate a significant difference (4% to 15%) in the number of fibers connecting ODCs, favoring pairs with alike rather than unalike ocular polarity. Here, we first examined whether these mesoscale features are also reflected in rs-FC between vertex pairs in human V1. Then, we extended our analysis to investigate the

heterogeneity of these features across different V1 subregions and their presence in interhemispheric rs-FC measurements.

3.1. Rs-FC between alike and unalike ODCs

Figure 2A illustrates the rs-FC levels, measured during the eyes-closed condition, for vertex pairs with alike and unalike ocular polarity as a function of distance between the two vertices of the pair. A two-way RM-ANOVA (distance and relative ocular polarity), applied to the measured rs-FC levels, revealed that rs-FC was significantly stronger between alike than unalike vertex pairs ($F(1, 10)=5.39$, $p=0.04$). Notably, while rs-FC decreased significantly with increasing distance between vertex pair ($F(9, 90)=25.56$, $p<10^{-3}$), the interaction between the effects of distance and relative ocular polarity remained non-significant ($F(9, 90)=1.34$, $p=0.28$). These results suggest that selective rs-FC between vertices with alike ocular polarity persists across relatively long distances.

The absence of interaction between the effects of distance and relative ocular polarity is also apparent in Figure 2B that illustrates the level of rs-FC selectivity, measured as rs-FC between alike – unalike vertex pairs, in each distance quantile. To make the rs-FC selectivity measurement similar to those in the previous anatomical studies [4,7], we normalized it relative to the overall level of rs-FC in the same quantile. As demonstrated here, rs-FC selectivity remained positive even at the highest tested distance quantile, where vertex pairs were approximately 35 mm apart, far exceeding the expected reach of a single horizontal fiber [1,5].

Notably, consistent with our previous reports in a smaller group of participants (Nasr et al., 2025), there was no significant difference between the number of vertices showing a preference for stimulation of the DE versus NDE ($p=0.18$) or their ODI ($p=0.23$) (Figure S2). Furthermore, a subsampling method assured us that the distance distribution was the same for alike and unalike vertex pairs (see Section 2.5.1). Thus, these findings cannot be attributed to an unbalanced distribution of ocular dominance activity in V1.

3.2. Reproducibility of rs-FC measurements across scan sessions

We tested whether the selective rs-FC between alike ODCs could be reliably detected across different days. Four individuals, selected based on availability, were re-scanned on a separate day using a different ultra-high-field MRI scanner and a modified data acquisition protocol (see Section 2.3.2). Here again, a three-way RM-ANOVA (distance, relative ocular polarity, and scan session) applied to the measured rs-

FC across different distance quantiles (Figure S4) confirmed robust effects of relative ocular polarity ($F(1, 3)=25.46$, $p=0.02$), and distance ($F(9, 27)=19.62$, $p=0.02$), while revealing no significant main effect of scan session ($F(1, 3)=0.69$, $p=0.47$) and no interactions between the effects of scan session and the other two factors ($p>0.18$). These results indicate that selective rs-FC between ODCs is highly reproducible over time and insensitive to scanner hardware and the exact acquisition parameters. Notably, the robustness of the ODC maps for our subjects has been tested and scrutinized in our previous studies [14,21].

3.3. Selectivity of rs-FC as a function of ODI and cortical depth

Studies in NHPs have suggested that ODI may influence the selectivity of horizontal fibers [4,7]. Accordingly, here, we tested the hypothesis that rs-FC depends not only on the relative ocular polarity of the vertex pair but also on their ODI. Furthermore, we tested whether the level of rs-FC varied across cortical depth levels, as suggested by animal models, and if rs-FC selectivity was detectable across all cortical depths. Considering the absence of significant interaction between the effects of relative ocular polarity and the distance between vertex pairs, data from all distance levels were averaged in all further analyses.

Figure 3A illustrates the rs-FC between vertex pairs as a function of their ODI, relative ocular polarity, and cortical depth (see Section 2.5). A three-way RM-ANOVA (relative ocular polarity, cortical depth, and ODI) revealed that rs-FC was significantly stronger between vertices with stronger ODIs than those with weaker ODIs ($F(4, 40)=8.78$, $p<0.01$) (Table S1). Here, a significant interaction between the effects of ODI and relative ocular polarity ($F(4, 40)=4.52$, $p=0.04$) demonstrated that rs-FC selectivity increases with the ODI of vertex pairs, reinforcing the link between functional connectivity and ocular dominance. This interaction is also apparent in Figure 3B that illustrates the level of rs-FC selectivity, measured as rs-FC between alike – unalike vertex pairs, without any normalization.

Moreover, consistent with the laminar organization of horizontal fibers in animals, rs-FC was highest in middle cortical depth compared to deeper and more superficial depths. This effect was particularly pronounced in regions with stronger ODIs, resulting in a significant interaction between the effects of ODI and cortical depth ($F(8, 80)=10.76$, $p<10^{-3}$). The lack of significant interaction between the effects of relative ocular polarity and cortical depth ($F(2, 20)=1.14$, $p=0.32$) suggests that rs-FC selectivity remains equivalent across cortical depths, thus ruling out the possibility that rs-FC selectivity was arbitrarily stronger simply because the ODC map was always sampled from deep cortical depth (to minimize the

430 blurring effect of pial veins). Similar results were also found after applying an LME model to the rs-FC
431 data (see supplementary analysis, and Table S2).

432 Together, these results suggest that the influence of relative ocular polarity and cortical depth is
433 contingent on higher ODIs. Considering the stronger fMRI signal in superficial compared to middle/deep
434 cortical depths (Figure 1D), these results also suggest that fMRI signal intensity does not dominate the
435 strength of rs-FC measured at different cortical depths. Instead, other factors, such as the organization of
436 horizontal fibers across cortical depths, may also influence the strength of rs-FC (see Discussion).

437

438 **3.4. Heterogeneity in rs-FC**

439 Multiple previous studies suggested stronger global visual processing and greater sensitivity to low spatial
440 frequency components —essential for global visual processing—in the lower compared to the upper
441 visual field [51–54]. Given that sensitivity to lower spatial frequency components requires sampling from a
442 larger visual field, it could be argued that rs-FC may be stronger in dorsal V1 subregions representing the
443 lower visual field compared to ventral V1 subregions representing the upper visual field. To test this
444 hypothesis, we divided V1 into two equivalent ROIs, representing the upper and lower portions of the
445 visual field (Figure 4A), and compared the rs-FC pattern across them.

446 Figure 4B illustrates the level of rs-FC measured in dorsal V1 (representing the lower visual field)
447 and ventral V1 (representing the upper visual field). Overall, consistent with our hypothesis, rs-FC was
448 stronger in the dorsal compared to ventral V1. Additionally, rs-FC selectivity was more uniform — i.e.,
449 independent of ODIs — in ventral compared to dorsal subregions (Figure 4C). A four-way RM-ANOVA
450 (ROI, relative ocular polarity, ODI, and cortical depth) (Table S3) applied to the measured rs-FC revealed
451 a significant main effect of ROI ($F(1, 10)=23.66$, $p<10^{-3}$), as well as significant interactions between the
452 effects of ROI and relative ocular polarity ($F(1, 10)=7.76$, $p=0.02$) and between the effects of ROI,
453 relative ocular polarity, and cortical depth ($F(2, 20)=5.02$, $p=0.03$) as well as between the effects of ROI,
454 ODI, and cortical depth ($F(8, 80)=3.65$, $p=0.03$). These findings indicate significant heterogeneity in both
455 the level of rs-FC and its selectivity across dorsal and ventral V1 subregions, as expected from the
456 differential visual processing mechanism in these regions.

457 A stronger preference for lower spatial frequency can also be found in V1 subregions representing
458 peripheral compared to central visual fields [55–57]. Accordingly, we further tested if a similar heterogeneity
459 can also be found between central and peripheral V1 subregions (Figure 5A). As demonstrated in Figure
460 5B, rs-FC was stronger in the peripheral compared to central V1 subregions across the superficial and
461 middle (but not deep) cortical depths. The same pattern, but less pronounced, was found for the selectivity

of rs-FC (Figure 5C). Here, the application of four-way RM-ANOVA (Table S4) to the measured rs-FC showed a significant interaction between the effects of ROI and cortical depth ($F(4, 40)=26.58$, $p=10^{-3}$). However, the two- and three-way interactions between the effects of ROI and relative ocular polarity remained non-significant ($F<0.33$, $p>0.58$). These results suggested that the overall pattern of rs-FC, its dependency on ODI, relative ocular polarity, and cortical depth may vary between V1 subregions, and that this heterogeneity appears to be consistent with the known biases in human visual perception across visual fields.

3.5. Interhemispheric rs-FC between ODCs

While monosynaptic callosal fibers directly linking V1 between hemispheres are limited [58], numerous polysynaptic connections — primarily through feedback pathways from other callosally connected visual areas (e.g., V2) — may contribute to interhemispheric rs-FC in V1. Consistently, multiple studies have already shown interhemispheric rs-FC between V1 subregions that represent the same portion of visual field [12,13]. Here, we extended those findings by examining the dependence of interhemispheric rs-FC connecting V1 subregions (dorsal vs. ventral and central vs. peripheral), on relative ocular polarity, ODI, and cortical depth. Because of the known retinotopic organization of interhemispheric connectivity, we limited our test to retinotopically corresponding areas, e.g., dorsal to dorsal and ventral to ventral V1.

As illustrated in Figure 6A, interhemispheric rs-FC exhibited striking regional differences between dorsal and ventral V1. First, similar to intrahemispheric rs-FC, dorsal V1 showed stronger interhemispheric rs-FC than ventral V1. Second, rs-FC selectivity (Figure 6B) followed distinct patterns in these subregions: in dorsal V1, vertex pairs with alike ocular polarity exhibited stronger rs-FC than those with unalike ocular polarity, whereas in ventral V1, this trend was reversed—rs-FC was stronger between vertex pairs with unalike ocular polarity than between those with alike ocular polarity. Consistently, a four-way RM-ANOVA (Table S5) revealed a significant main effect of ROI ($F(1, 10)=25.84$, $p<10^{-3}$) and significant three-way interactions between the effects of ROI, relative ocular polarity, and ODI ($F(4, 40)=4.66$, $p=0.03$) as well as between ROI, ODI and cortical depth ($F(2, 20)=3.30$, $p=0.04$).

Heterogeneous rs-FC was also observed when comparing interhemispheric rs-FC between central and peripheral V1 subregions. Specifically, again similar to intrahemispheric rs-FC, the relationship between rs-FC and cortical depth varied between central and peripheral regions (Figure 7A). Moreover, the overall pattern of rs-FC selectivity also differed— in the peripheral subregion, selectivity was more pronounced in superficial depths, favoring vertex pairs with alike ocular polarity (Figure 7B). In contrast, in the

central subregion, we observed a weaker but opposite trend, with a slight preference for ODCs with unalike ocular polarity. A four-way RM-ANOVA on the measured rs-FC (Table S6) revealed a significant interaction between the effect of ROI and cortical depth ($F(2, 20)=21.53$, $p<10^{-3}$), as well as a significant three-way interaction between the effect of ROI, relative ocular polarity, and cortical depth ($F(2, 20)=4.30$, $p=0.03$).

These findings demonstrate that, like intrahemispheric rs-FC, interhemispheric V1 rs-FC is not uniform but instead varies systematically across V1 subregions, aligning with their specialized roles in visual processing. Moreover, the striking differences between intrahemispheric and interhemispheric rs-FC patterns suggest that these two forms of functional connectivity may be under the influence of distinct anatomical and functional neuronal mechanisms.

3.6. Relating ODC maps to rs-FC

Our findings suggest that for each vertex, the relative ocular polarity and the ODI of surrounding vertices may be related to (and even predictable based on) corresponding rs-FC measures. To rigorously test this hypothesis (H1), we pseudo-randomly selected 1,000 seed vertices (10.91% ± 1.87% of all vertices within our V1 ROI) in each hemisphere (see Section 2.5), generated their 2D rs-FC map with the other vertices, and quantified the correlation between the resultant rs-FC map and the ODC map centered around the seed point. To mitigate the influence of the fMRI signal's PSF, we excluded the inner 3 mm radius from our analysis (Figure 8A). We varied the outer radius from 4 to 10 mm in 0.5 mm increments and compared the measured correlation values against a stringent baseline, defined as the correlation between the same rs-FC pattern and a randomly selected, non-overlapping portion of the ODC map from the same V1 area ($H0_a$). These analyses were conducted separately for rs-FC measured within deep, middle, and superficial cortical depths.

As shown in Figure 8B, although the correlation between ODC and rs-FC maps decreased as the outer radius expanded, it remained higher than either baseline measure across all cortical depths. A three-way RM-ANOVA (measurement type (H1 vs. $H0_a$), outer radius, cortical depth), applied to the measured correlation values yielded a significant effect of outer radius ($F(12,120)=569.17$, $p<10^{-10}$) and measurement type ($F(1, 10)=63.70$, $p<10^{-3}$), with a marginal interaction between the two effects ($F(12, 120)=2.77$, $p=0.07$). There was no significant main effect of cortical depth ($p=0.41$) or significant interaction between the effect of cortical depth and the other two independent factors ($p>0.32$), indicating that the predictive relationship between rs-FC and ODC organization holds across different cortical depths.

It has already been shown that the organization of ODCs may vary based on eccentricity in the visual field [59]. Given this possibility, it could be argued that the change in the location of the baseline disc could affect the measured correlation values, depending on the distance relative to the actual disc. To rule out this possibility, we conducted a control analysis using an alternative baseline in which the ODC map was only rotated 180° before computing its correlation with the rs-FC pattern ($H0_b$). In this condition, the ODC and rs-FC rings remain overlapping relative to each other. Even under this control condition, an RM-ANOVA confirmed robust effects of outer radius ($F(12,120)=724.01$, $p<10^{-11}$), measurement type ($F(1, 10)=81.76$, $p<10^{-4}$), and the significant interaction between the effects of outer radius and measurement type ($F(12, 120)=10.53$), $p<0.01$). The cortical depth showed no significant main or interaction effect with the other factors ($p>0.14$), reinforcing the robustness of our findings across cortical depths.

These results provide empirical support for the hypothesis that rs-FC patterns contain specific information about ODC organization, despite being derived from independent datasets collected in separate scan sessions. The persistence of this relationship across cortical depths and under rigorous control conditions underscores the fundamental link between rs-FC and the underlying columnar architecture of V1.

4. Discussion

Rs-FC has been extensively used to investigate functional connections between predefined macroscale brain regions, primarily at the spatial scale of brain areas [60,61], or to segment the brain into multiple co-fluctuating regions [62–64]. In this study, we provide compelling functional evidence for the selective rs-FC between ODCs — the building blocks of neuronal processing in V1. Our findings reveal key aspects of the mesoscale functional organization of V1, emphasizing heterogeneities across cortical depth and subregions, and offer a fresh perspective on its interhemispheric functional connectivity. Furthermore, we demonstrate new evidence for the predictability of ODC maps based on their rs-FC.

4.1. Consistency between rs-FC pattern and anatomical connections

Our findings provide some of the first functional evidence of significantly stronger rs-FC between ODCs with alike compared to those with unalike ocular polarity, in humans, aligning with prior animal studies using postmortem histological methods [4,7,65] as well as optical imaging and electrophysiological recordings [8–11]. Furthermore, the observation that rs-FC is strongest in middle cortical layers—compared

557 to deep and superficial layers—closely aligns with neuroanatomical studies that demonstrated the highest
558 prevalence of horizontal fibers in layer 4B [3].

559 Despite the methodological differences between rs-FC and histological techniques based on using
560 tracers, the overall level of rs-FC, and the level of rs-FC selectivity reported here (Figure 2B) is also
561 comparable to the quantitative measure of this selectivity based on anatomical techniques. Specifically,
562 three previous studies have reported 4% [4], 8% [65], and 15% [7] difference in the number of horizontal fibers
563 connecting ODCs with alike rather than unalike relative ocular polarity. Given that at least two of these
564 studies used the same tracer (biocytin) to detect the horizontal fibers [4,7], the difference in the level of
565 selectivity is at least partly due to between-species (macaque nemestrina vs. macaque fascicularis) and
566 between-individual variability.

567 Beyond these functional parallels to structural measurements, our results highlight a strong influence
568 of ODI on rs-FC strength. This effect was robustly detected despite rs-FC and ODI being measured
569 during separate scans collected on different days. Notably, while the previous anatomical studies
570 suggested that the selectivity of horizontal connections is higher in sites that show a stronger ODI [4,7], to
571 our knowledge, the link between ODI and the level of rs-FC has never been explicitly tested in animal
572 studies.

573

574 **4.2.The impact of common input on rs-FC**

575 Common input can shape the overall pattern of rs-FC [66]. It is known that rs-FC may adapt to the shape of
576 visual stimuli [67,68]. To minimize the impact of visual input on rs-FC, we instructed participants to keep
577 their eyes closed during resting-state fMRI scans. While this approach significantly reduces the impact of
578 common sensory input, one could still argue that relayed spontaneous activity into V1 via feedforward
579 connections from the lateral geniculate nucleus (LGN) might still contribute to the selective rs-FC
580 observed between ODCs with similar ocular polarity.

581 Although input from the LGN may play a role in generating spontaneous activity within V1, this
582 input follows a strict visuotopic organization [69]. Given that rs-FC selectivity was robustly detected over
583 large cortical distances—well beyond the receptive fields of individual V1 columns—the LGN is unlikely
584 to be the primary driver of this phenomenon, particularly at these larger spatial scales [8,12]. Additionally, to
585 eliminate potential confounds from the fMRI PSF, we excluded vertex pairs separated by less than 3 mm.
586 This process also reduced the residual impact of LGN input on the V1 rs-FC pattern.

587

588

589 **4.3. Contribution of polysynaptic connectivity and synchronous neuronal activity to rs-FC**

590 Given these similarities, it is compelling to link the observed rs-FC patterns to the organization of
591 horizontal fibers. While the spatial organization of rs-FC is thought to be at least partially shaped by
592 underlying anatomical connections [61,70–72], rs-FC is not merely a passive reflection of monosynaptic
593 anatomical connectivity [73]. Instead, the existence of polysynaptic connections and synchronous neuronal
594 activity across ODCs play crucial roles in shaping rs-FC.

595 The role of polysynaptic connections in generating rs-FC between sites that are not directly connected
596 has been well established [44,73–76]. This influence is also evident in our findings, which reveal rs-FC
597 between vertex pairs separated by distances of up to 35 mm (Figure 2), far exceeding the reach of a
598 monosynaptic horizontal connection of up to 8mm [1,4,5]. Crucially, our results provide direct evidence that
599 rs-FC selectivity is preserved even across polysynaptic pathways.

600 Beyond structural connectivity, mounting evidence suggests that rs-FC strength depends on the
601 amplitude of synchronous gamma-band neural activity between the seeded and targeted sites [74,77–80].
602 Notably, the first direct evidence of such synchronous activity came from simultaneous single-unit
603 recordings from V1 columns that share ocular [8–10] and orientation [9,10,81,82] preference—even when these
604 columns are spatially distant and have non-overlapping receptive fields.

605 Together, these results strongly support the hypothesis that polysynaptic connections within the visual
606 cortex play a crucial role beyond local visual processing. These connections may be instrumental in
607 integrating information across a large visual field, contributing to a more coherent visual perception [81].

608

609 **4.4. Heterogeneity**

610 Previous studies have shown that global stimulus configuration is more prominent in the lower than in the
611 upper visual field [51,54,83]. Neuroimaging research further reveals that dorsal cortical regions, representing
612 the lower visual field, exhibit heightened sensitivity to visual features critical for global configuration
613 encoding, such as lower spatial frequencies [52].

614 Extending these findings, we showed that rs-FC is significantly stronger in dorsal compared to ventral
615 V1 subregions and in peripheral compared to central V1 subregions. Notably, these effects hold for both
616 intrahemispheric and interhemispheric rs-FC (see also Section 4.5). This pattern aligns with the well-
617 established higher sensitivity for lower spatial frequencies in dorsal versus ventral [53,84,85] and in peripheral
618 vs. central V1 subregions [55–57].

Importantly, these findings cannot be explained by variations in gradient-echo BOLD signal intensity across these regions. To clarify, the BOLD signal is generally stronger in the superficial compared to middle and deep cortical depths (Figure 1C) and in central compared to peripheral V1 regions. Yet, rs-FC was strongest in the middle cortical depths and in peripheral V1 subregions, indicating that the observed connectivity patterns are not merely a byproduct of BOLD signal strength. Instead, these results highlight the fundamental role of V1 functional architecture in shaping rs-FC, independent of signal intensity biases.

While our findings on the overall rs-FC pattern across V1 subregions align with the well-established heterogeneity in visual processing across visual fields, their direct link to visual perception remains uncertain without behavioral measurements. Future studies are essential to rigorously assess this connection.

4.5. Interhemispheric connections and their role

Interhemispheric FC is crucial for spatial integration around the vertical meridian. Despite its fundamental role in visual perception, our understanding of V1 interhemispheric FC remains limited. This gap in knowledge stems from earlier findings that, compared to downstream areas like V2, the callosal fibers linking the contralateral V1s are sparse and largely confined to a narrow zone along the V1-V2 border [58,86,87]. Given this and considering that V1 receives extensive feedback from V2—a binocular visual area with robust interhemispheric connections—it is logical to assume that interhemispheric rs-FC in V1 should lack selectivity for ODCs.

Our results overturn this assumption. We demonstrate that, particularly in more peripheral and dorsal regions, rs-FC remains significantly stronger between ODCs with alike rather than unalike ocular polarity. This raises two key possibilities: first, despite their limited numbers, V1 callosal connections may still facilitate selective rs-FC between ODCs in opposite hemispheres. Second, the pronounced rs-FC selectivity in superficial cortical layers is consistent with the hypothesis that indirect pathways, mediated by feedback connections from callosally-connected downstream areas, contribute to this phenomenon. Yet, it remains unclear how the eye-of-origin information persists within an indirect, polysynaptic network through binocular visual areas. Resolving this will be essential for understanding the mechanisms underlying interhemispheric functional organization in V1.

4.6. Mapping ODCs based on rs-FC

Our findings demonstrate that the organization of ODCs and ODI have a direct influence on the pattern of rs-FC across V1. We also provide evidence suggesting a significant relationship between ODC maps and the rs-FC pattern [11], marking the first step toward leveraging rs-FC for potential segmentation of the visual cortex at mesoscale levels (see also [18] for a similar approach outside the visual cortex).

This said, ODI alone is unlikely to drive the rs-FC pattern. Prior studies in NHPs suggest that orientation and wavelength (color) preference also modulate functional connectivity between cortical columns [9–11,81,82,88]. Consequently, accurately predicting ODC maps from rs-FC requires disentangling the distinct contributions of these factors on the rs-FC pattern. Future research must refine this approach to fully harness the potential of rs-FC in visual cortex mapping.

4.7. Limitation

Although we leveraged an advanced fMRI technique with relatively high spatial resolution, our measurements only indirectly reflect neuronal activity mediated by the BOLD effect and are based on correlations (rather than causal inference). These measurements remain susceptible to partial voluming effects, which constrain our ability to precisely assess rs-FC across cortical depth levels. Additionally, the inherent sensitivity of our fMRI method to pial veins results in stronger yet partially blurred signals in more superficial cortical depths [14,38–40].

These challenges, compounded by the lack of visible landmarks to detect the laminar organization of the visual cortex in vivo, hindered our ability to accurately assess the laminar-specific rs-FC. This limitation may explain the insignificant impact of cortical depth on rs-FC selectivity in our results, despite the reports from anatomical studies in animals that the selective connectivity between ODCs is more apparent in superficial (layer 2/3) compared to middle (layer 4B) cortical depths [3]. Future studies employing cutting-edge techniques with higher spatial resolution and reduced sensitivity to vascular effects are crucial to fully uncover the precise laminar profile of rs-FC.

5. Conclusion

The introduction of higher-performance MRI scanners and technological advancements in hardware and software design enable us to now resolve neuronal responses at the fine spatial scale of cortical columns. This study demonstrates the power of high-resolution fMRI in capturing one of the most fine-grained features of cortical organization including the selective connectivity between ODCs. Given that this

selectivity produces only a modest 4% to 15% difference in horizontal fiber density, our findings underscore the remarkable sensitivity of high-resolution fMRI in revealing the mesoscale functional organization of the human visual system. Thanks to the short duration of a resting-state scan session (<30 mins) compared to the time necessary for localizing ODCs based on dichoptic visual stimulation (~3-4 hours [21]) and the absence of cognitive load on the participant, the mesoscale rs-FC measurements present a potentially powerful tool for clinicians to assess visual system integrity at the mesoscale level. It may even enable such studies for the first time in patients where conventional methods of ODC mapping are impractical or impossible (e.g., in monocularly blind individuals).

690 # References

691 1. Fisken, R. A., Garey, L. J. & Powell, T. P. The intrinsic, association and commissural
692 connections of area 17 on the visual cortex. *Philos. Trans. R. Soc. Lond. B. Biol. Sci.*
693 **272**, 487–536 (1975).
694 2. Gilbert, C. D. & Wiesel, T. N. Morphology and intracortical projections of functionally
695 characterised neurones in the cat visual cortex. *Nature* **280**, 120–125 (1979).
696 3. Rockland, K. S. & Lund, J. S. Intrinsic laminar lattice connections in primate visual
697 cortex. *J. Comp. Neurol.* **216**, 303–318 (1983).
698 4. Yoshioka, T., Blasdel, G. G., Levitt, J. B. & Lund, J. S. Relation between patterns of
699 intrinsic lateral connectivity, ocular dominance, and cytochrome oxidase-reactive
700 regions in macaque monkey striate cortex. *Cereb. Cortex N. Y. N 1991* **6**, 297–310
701 (1996).
702 5. Angelucci, A. *et al.* Circuits for local and global signal integration in primary visual
703 cortex. *J. Neurosci. Off. J. Soc. Neurosci.* **22**, 8633–8646 (2002).
704 6. Lund, J. S., Angelucci, A. & Bressloff, P. C. Anatomical substrates for functional
705 columns in macaque monkey primary visual cortex. *Cereb. Cortex N. Y. N 1991* **13**, 15–
706 24 (2003).
707 7. Malach, R., Amir, Y., Harel, M. & Grinvald, A. Relationship between intrinsic
708 connections and functional architecture revealed by optical imaging and in vivo
709 targeted biocytin injections in primate striate cortex. *Proc. Natl. Acad. Sci. U. S. A.* **90**,
710 10469–10473 (1993).
711 8. Chiu, C. & Weliky, M. Relationship of Correlated Spontaneous Activity to Functional
712 Ocular Dominance Columns in the Developing Visual Cortex. *Neuron* **35**, 1123–1134
713 (2002).
714 9. Omer, D. B., Fekete, T., Ulchin, Y., Hildesheim, R. & Grinvald, A. Dynamic Patterns of
715 Spontaneous Ongoing Activity in the Visual Cortex of Anesthetized and Awake Monkeys
716 are Different. *Cereb. Cortex* **29**, 1291–1304 (2019).

10. Ts'o, D. Y., Gilbert, C. D. & Wiesel, T. N. Relationships between horizontal interactions and functional architecture in cat striate cortex as revealed by cross-correlation analysis. *J. Neurosci. Off. J. Soc. Neurosci.* **6**, 1160–1170 (1986).
11. Cai, X. *et al.* Mesoscale functional connectivity in macaque visual areas. *NeuroImage* **271**, 120019 (2023).
12. Dawson, D. A. *et al.* Partial Correlation-Based Retinotopically Organized Resting-State Functional Connectivity Within and Between Areas of the Visual Cortex Reflects More Than Cortical Distance. *Brain Connect.* **6**, 57–75 (2016).
13. Mendola, J. D., Lam, J., Rosenstein, M., Lewis, L. B. & Shmuel, A. Partial correlation analysis reveals abnormal retinotopically organized functional connectivity of visual areas in amblyopia. *NeuroImage Clin.* **18**, 192–201 (2018).
14. Nasr, S., Polimeni, J. R. & Tootell, R. B. Interdigitated Color- and Disparity-Selective Columns within Human Visual Cortical Areas V2 and V3. *J Neurosci* **36**, 1841–57 (2016).
15. Tootell, R. B. & Nasr, S. Scotopic Vision Is Selectively Processed in Thick-Type Columns in Human Extrastriate Cortex. *Cereb. Cortex* **31**, 1163–1181 (2021).
16. Kennedy, B., Bex, P., Hunter, D. G. & Nasr, S. Two fine-scale channels for encoding motion and stereopsis within the human magnocellular stream. *Prog. Neurobiol.* **220**, 102374 (2023).
17. Ai, H., Lin, W., Liu, C., Chen, N. & Zhang, P. Mesoscale functional organization and connectivity of color, disparity, and naturalistic texture in human second visual area. *eLife* **13**, (2025).
18. Huber, L. *et al.* Layer-dependent functional connectivity methods. *Prog. Neurobiol.* **207**, 101835 (2021).
19. Cheng, K., Waggoner, R. A. & Tanaka, K. Human ocular dominance columns as revealed by high-field functional magnetic resonance imaging. *Neuron* **32**, 359–374 (2001).

20. Menon, R. S., Ogawa, S., Strupp, J. P. & Uğurbil, K. Ocular dominance in human V1 demonstrated by functional magnetic resonance imaging. *J. Neurophysiol.* **77**, 2780–2787 (1997).
21. Nasr, S. *et al.* Differential impacts of strabismic and anisometropic amblyopia on the mesoscale functional organization of the human visual cortex. *J. Neurosci.* (2025) doi:10.1523/JNEUROSCI.0745-24.2024.
22. Yacoub, E., Shmuel, A., Logothetis, N. & Uğurbil, K. Robust detection of ocular dominance columns in humans using Hahn Spin Echo BOLD functional MRI at 7 Tesla. *NeuroImage* **37**, 1161–1177 (2007).
23. Aganj, I. & Nasr, S. Selective Functional Connectivity between Ocular Dominance Columns in the Primary Visual Cortex. in *Ophthalmic Medical Image Analysis* (eds. Bhavna, A., Chen, H., Fang, H., Fu, H. & Lee, C. S.) 1–10 (Springer Nature Switzerland, Cham, 2024). doi:10.1007/978-3-031-73119-8_1.
24. Sereno, M. I. *et al.* Borders of multiple visual areas in humans revealed by functional magnetic resonance imaging. *Science* **268**, 889–93 (1995).
25. Tootell, R. B. *et al.* Functional analysis of V3A and related areas in human visual cortex. *J Neurosci* **17**, 7060–78 (1997).
26. Mareyam, A., Kirsch, J. E., Chang, Y., Madan, G. & Wald, L. L. A 64-Channel 7T array coil for accelerated brain MRI. in vol. 764 (2020).
27. Polimeni, J. R. *et al.* Reducing sensitivity losses due to respiration and motion in accelerated echo planar imaging by reordering the autocalibration data acquisition. *Magn Reson Med* (2015) doi:10.1002/mrm.25628.
28. Hoge, W. S. & Polimeni, J. R. Dual-polarity GRAPPA for simultaneous reconstruction and ghost correction of echo planar imaging data. *Magn. Reson. Med.* **76**, 32–44 (2016).
29. Webb, A. G. & Collins, C. M. Parallel transmit and receive technology in high-field magnetic resonance neuroimaging. *Int. J. Imaging Syst. Technol.* **20**, 2–13 (2010).
30. Wrede, K. H. *et al.* Caudal image contrast inversion in MPRAGE at 7 Tesla: problem and solution. *Acad. Radiol.* **19**, 172–178 (2012).
31. Fischl, B. FreeSurfer. *Neuroimage* **62**, 774–81 (2012).

773 32. Dale, A. M., Fischl, B. & Sereno, M. I. Cortical surface-based analysis. I. Segmentation
774 and surface reconstruction. *Neuroimage* **9**, 179–94 (1999).
775 33. Wang, J., Nasr, S., Roe, A. W. & Polimeni, J. R. Critical factors in achieving fine-scale
776 functional MRI: Removing sources of inadvertent spatial smoothing. *Hum. Brain Mapp.*
777 **43**, 3311–3331 (2022).
778 34. Greve, D. N. & Fischl, B. Accurate and robust brain image alignment using boundary-
779 based registration. *Neuroimage* **48**, 63–72 (2009).
780 35. Moeller, S. *et al.* NOise reduction with DIstribution Corrected (NORDIC) PCA in dMRI
781 with complex-valued parameter-free locally low-rank processing. *Neuroimage* **226**,
782 117539 (2021).
783 36. Chen, J. E., Jahanian, H. & Glover, G. H. Nuisance Regression of High-Frequency
784 Functional Magnetic Resonance Imaging Data: Denoising Can Be Noisy. *Brain*
785 *Connect.* **7**, 13–24 (2017).
786 37. Blazejewska, A. I., Fischl, B., Wald, L. L. & Polimeni, J. R. Intracortical smoothing of
787 small-voxel fMRI data can provide increased detection power without spatial
788 resolution losses compared to conventional large-voxel fMRI data. *Neuroimage* **189**,
789 601–614 (2019).
790 38. De Martino, F. *et al.* Cortical depth dependent functional responses in humans at 7T:
791 improved specificity with 3D GRASE. *PLoS One* **8**, e60514 (2013).
792 39. Koopmans, P. J., Barth, M. & Norris, D. G. Layer-specific BOLD activation in human V1.
793 *Hum. Brain Mapp.* **31**, 1297–1304 (2010).
794 40. Polimeni, J. R., Fischl, B., Greve, D. N. & Wald, L. L. Laminar analysis of 7T BOLD using
795 an imposed spatial activation pattern in human V1. *Neuroimage* **52**, 1334–46 (2010).
796 41. Tootell, R., Hamilton, S., Silverman, M. & Switkes, E. Functional anatomy of macaque
797 striate cortex. I. Ocular dominance, binocular interactions, and baseline conditions. *J.*
798 *Neurosci.* **8**, 1500–1530 (1988).
799 42. Engel, S. A., Glover, G. H. & Wandell, B. A. Retinotopic organization in human visual
800 cortex and the spatial precision of functional MRI. *Cereb Cortex* **7**, 181–92 (1997).

43. Olman, C., Van de Moortele, P. & Ugurbil, K. Point spread function for gradient echo and spin echo BOLD fMRI at 7 Tesla. in 1066 (2004).
44. Shmuel, A., Yacoub, E., Chaimow, D., Logothetis, N. K. & Ugurbil, K. Spatio-temporal point-spread function of fMRI signal in human gray matter at 7 Tesla. *Neuroimage* **35**, 539–552 (2007).
45. Bi, H. *et al.* Neuronal responses in visual area V2 (V2) of macaque monkeys with strabismic amblyopia. *Cereb. Cortex N. Y. N 1991* **21**, 2033–2045 (2011).
46. Crawford, M. L. & von Noorden, G. K. The effects of short-term experimental strabismus on the visual system in Macaca mulatta. *Invest. Ophthalmol. Vis. Sci.* **18**, 496–505 (1979).
47. Hubel, D. H. & Wiesel, T. N. Receptive fields, binocular interaction and functional architecture in the cat's visual cortex. *J. Physiol.* **160**, 106–154 (1962).
48. Kiorpes, L., Kiper, D. C., O'Keefe, L. P., Cavanaugh, J. R. & Movshon, J. A. Neuronal correlates of amblyopia in the visual cortex of macaque monkeys with experimental strabismus and anisometropia. *J. Neurosci. Off. J. Soc. Neurosci.* **18**, 6411–6424 (1998).
49. Aganj, I., Yeo, B. T. T., Sabuncu, M. R. & Fischl, B. On removing interpolation and resampling artifacts in rigid image registration. *IEEE Trans. Image Process.* **22**, 816–827 (2012).
50. Halton, J. H. On the efficiency of certain quasi-random sequences of points in evaluating multi-dimensional integrals. *Numer. Math.* **2**, 84–90 (1960).
51. Christman, S. D. Local-global processing in the upper versus lower visual fields. *Bull. Psychon. Soc.* **31**, 275–278 (1993).
52. Nasr, S. & Tootell, R. B. H. Asymmetries in Global Perception Are Represented in Near- versus Far-Preferring Clusters in Human Visual Cortex. *J. Neurosci. Off. J. Soc. Neurosci.* **40**, 355–368 (2020).
53. Niebauer, C. L. & Christman, S. D. Upper and lower visual field differences in categorical and coordinate judgments. *Psychon. Bull. Rev.* **5**, 147–151 (1998).

54. Previc, F. H. Functional specialization in the lower and upper visual fields in humans: Its ecological origins and neurophysiological implications. *Behav. Brain Sci.* **13**, 519–542 (1990).
55. De Valois, R. L., Albrecht, D. G. & Thorell, L. G. Spatial frequency selectivity of cells in macaque visual cortex. *Vision Res.* **22**, 545–559 (1982).
56. Schiller, P. H., Finlay, B. L. & Volman, S. F. Quantitative studies of single-cell properties in monkey striate cortex. III. Spatial frequency. *J. Neurophysiol.* **39**, 1334–1351 (1976).
57. Tootell, R. B., Silverman, M. S., Hamilton, S. L., Switkes, E. & De Valois, R. L. Functional anatomy of macaque striate cortex. V. Spatial frequency. *J. Neurosci. Off. J. Soc. Neurosci.* **8**, 1610–1624 (1988).
58. Kennedy, H., Dehay, C. & Bullier, J. Organization of the callosal connections of visual areas V1 and V2 in the macaque monkey. *J. Comp. Neurol.* **247**, 398–415 (1986).
59. Adams, D. L., Sincich, L. C. & Horton, J. C. Complete pattern of ocular dominance columns in human primary visual cortex. *J. Neurosci. Off. J. Soc. Neurosci.* **27**, 10391–10403 (2007).
60. Biswal, B., Zerrin Yetkin, F., Haughton, V. M. & Hyde, J. S. Functional connectivity in the motor cortex of resting human brain using echo-planar mri. *Magn. Reson. Med.* **34**, 537–541 (1995).
61. Fox, M. D. & Raichle, M. E. Spontaneous fluctuations in brain activity observed with functional magnetic resonance imaging. *Nat. Rev. Neurosci.* **8**, 700–711 (2007).
62. Power, J. D. *et al.* Functional Network Organization of the Human Brain. *Neuron* **72**, 665–678 (2011).
63. Yeo, B. T. *et al.* The organization of the human cerebral cortex estimated by intrinsic functional connectivity. *J. Neurophysiol.* **106**, 1125–1165 (2011).
64. Gordon, E. M. *et al.* Generation and Evaluation of a Cortical Area Parcellation from Resting-State Correlations. *Cereb. Cortex* **26**, 288–303 (2016).
65. Tychsen, L., Wong, A. M.-F. & Burkhalter, A. Paucity of horizontal connections for binocular vision in V1 of naturally strabismic macaques: Cytochrome oxidase compartment specificity. *J. Comp. Neurol.* **474**, 261–275 (2004).

858 66. Adams, P. *et al.* Corticothalamic interactions in the transfer of visual information.
859 *Philos. Trans. R. Soc. Lond. B. Biol. Sci.* **357**, 1739–1752 (2002).
860 67. Nasr, S., Kleinfeld, D. & Polimeni, J. R. The Global Configuration of Visual Stimuli Alters
861 Co-Fluctuations of Cross-Hemispheric Human Brain Activity. *J. Neurosci. Off. J. Soc.*
862 *Neurosci.* **41**, 9756–9766 (2021).
863 68. Ontivero-Ortega, M. *et al.* Intra-V1 functional networks and classification of observed
864 stimuli. *Front. Neuroinformatics* **18**, 1080173 (2024).
865 69. Blasdel, G. G. & Lund, J. S. Termination of afferent axons in macaque striate cortex. *J.*
866 *Neurosci. Off. J. Soc. Neurosci.* **3**, 1389–1413 (1983).
867 70. De Luca, M., Beckmann, C. F., De Stefano, N., Matthews, P. M. & Smith, S. M. fMRI
868 resting state networks define distinct modes of long-distance interactions in the
869 human brain. *NeuroImage* **29**, 1359–1367 (2006).
870 71. van den Heuvel, M. P., Mandl, R. C. W., Kahn, R. S. & Hulshoff Pol, H. E. Functionally
871 linked resting-state networks reflect the underlying structural connectivity architecture
872 of the human brain. *Hum. Brain Mapp.* **30**, 3127–3141 (2009).
873 72. Wang, Z. *et al.* The relationship of anatomical and functional connectivity to resting-
874 state connectivity in primate somatosensory cortex. *Neuron* **78**, 1116–1126 (2013).
875 73. Honey, C. J. *et al.* Predicting human resting-state functional connectivity from
876 structural connectivity. *Proc. Natl. Acad. Sci. U. S. A.* **106**, 2035–2040 (2009).
877 74. Shmuel, A. & Leopold, D. A. Neuronal correlates of spontaneous fluctuations in fMRI
878 signals in monkey visual cortex: Implications for functional connectivity at rest. *Hum.*
879 *Brain Mapp.* **29**, 751–761 (2008).
880 75. Adachi, Y. *et al.* Functional connectivity between anatomically unconnected areas is
881 shaped by collective network-level effects in the macaque cortex. *Cereb. Cortex N. Y.*
882 *N 1991* **22**, 1586–1592 (2012).
883 76. Frau-Pascual, A., Fogarty, M., Fischl, B., Yendiki, A. & Aganj, I. Quantification of
884 structural brain connectivity via a conductance model. *NeuroImage* **189**, 485–496
885 (2019).

886 77. Mateo, C., Knutsen, P. M., Tsai, P. S., Shih, A. Y. & Kleinfeld, D. Entrainment of Arteriole
887 Vasomotor Fluctuations by Neural Activity Is a Basis of Blood-Oxygenation-Level-
888 Dependent 'Resting-State' Connectivity. *Neuron* **96**, 936-948.e3 (2017).
889 78. Nir, Y. *et al.* Coupling between neuronal firing rate, gamma LFP, and BOLD fMRI is
890 related to interneuronal correlations. *Curr. Biol. CB* **17**, 1275–1285 (2007).
891 79. Scheeringa, R. *et al.* Neuronal dynamics underlying high- and low-frequency EEG
892 oscillations contribute independently to the human BOLD signal. *Neuron* **69**, 572–583
893 (2011).
894 80. Schölvinck, M. L., Maier, A., Ye, F. Q., Duyn, J. H. & Leopold, D. A. Neural basis of global
895 resting-state fMRI activity. *Proc. Natl. Acad. Sci. U. S. A.* **107**, 10238–10243 (2010).
896 81. Gilbert, C. D. & Wiesel, T. N. Columnar specificity of intrinsic horizontal and
897 corticocortical connections in cat visual cortex. *J. Neurosci. Off. J. Soc. Neurosci.* **9**,
898 2432–2442 (1989).
899 82. Sincich, L. C. & Blasdel, G. G. Oriented Axon Projections in Primary Visual Cortex of the
900 Monkey. *J. Neurosci.* **21**, 4416–4426 (2001).
901 83. Levine, M. W. & McAnany, J. J. The relative capabilities of the upper and lower visual
902 hemifields. *Vision Res.* **45**, 2820–2830 (2005).
903 84. Skrandies, W. The Upper and Lower Visual Field of Man: Electrophysiological and
904 Functional Differences. in *Progress in Sensory Physiology* (eds. Autrum, H. et al.) 1–93
905 (Springer, Berlin, Heidelberg, 1987). doi:10.1007/978-3-642-71060-5_1.
906 85. Thomas, N. A. & Elias, L. J. Upper and lower visual field differences in perceptual
907 asymmetries. *Brain Res.* **1387**, 108–115 (2011).
908 86. Caspers, S. *et al.* Target sites for transcallosal fibers in human visual cortex – A
909 combined diffusion and polarized light imaging study. *Cortex* **72**, 40–53 (2015).
910 87. Clarke, S. & Miklossy, J. Occipital cortex in man: organization of callosal connections,
911 related myelo- and cytoarchitecture, and putative boundaries of functional visual
912 areas. *J. Comp. Neurol.* **298**, 188–214 (1990).
913 88. Livingstone, M. S. & Hubel, D. H. Specificity of intrinsic connections in primate primary
914 visual cortex. *J. Neurosci. Off. J. Soc. Neurosci.* **4**, 2830–2835 (1984).

Acknowledgment

This work was supported by the National Eye Institute (R01EY030434 and R01EY029713), the National Institute on Aging (RF1AG068261), the Deutsche Forschungsgemeinschaft (DFG, German Research Foundation) – project no. 347592254 (WE 5046/4-2 and/or KI 1337/2-2), the Federal Ministry of Education and Research (BMBF) under support code 01ED2210, as well as by the MGH/HST Athinoula A. Martinos Center for Biomedical Imaging. Crucial imaging resources were made available by the NIH Shared Instrumentation Grant S10RR019371. We thank Azma Mareyam for helping with hardware maintenance as well as John Kirsch and Daniel Park for their support in raw data export during this study. We thank Amanda Nabasaliza, Sarala N. Malladi, and Bryan Kennedy for their help with recruitment and data collection. We also thank Drs. Antony Morland and Jingyuan Chen for their comments.

Author's contribution

Conceptualization, formal analysis, visualization, writing – original draft: M.E.S., I.A. and S.N.

Investigation, writing – review & editing: M.E.S., I.A., J.S., B.B., Y.C., W.S.H., E.K., N.W. and S.N.

Methodology, software: M.E.S., I.A., J.S., B.B., Y.C., W.S.H. and S.N.

Data curation, validation: M.E.S. and S.N. Supervision: E.K., N.W. and S.N.

Funding acquisition: N.W. and S.N.

Resources, project administration: S.N.

Figures

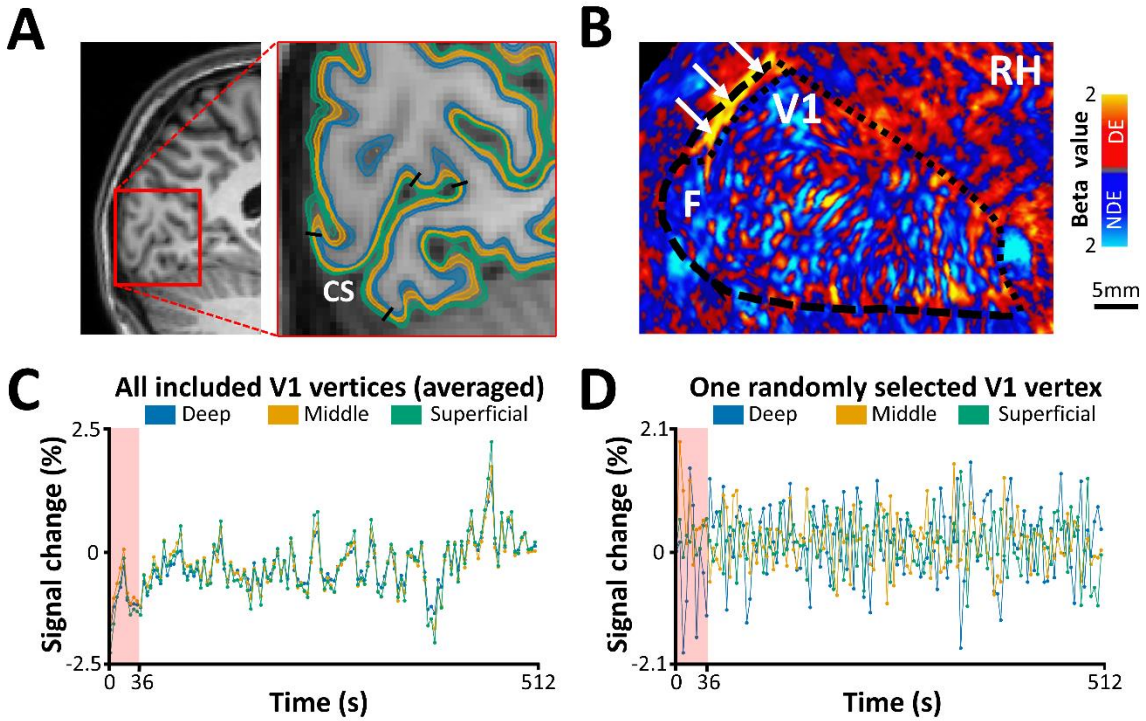

Figure 1. Structural and functional MRI from one individual participant. **A)** Reconstruction of cortical surfaces at different depth levels. For each participant, V1 was localized retinotopically along the calcarine sulcus (CS). As a part of brain reconstruction, the cortical gray matter was divided into deep (blue), middle (orange), and superficial (green) depths with small gaps between them (see Methods). **B)** Differential ODC map (beta values) overlaid on the flattened cortex. The ocular dominance response was derived by contrasting the response to stimulation of the dominant eye (DE; red to yellow) versus the non-dominant eye (NDE; blue to cyan). The map shows the stimulated portion of V1 (radius<10º) in the right hemisphere (RH) of a representative subject. Notably, a large activity patch along the dorsal part of the vertical meridian (white arrows), in which the ODCs could not be mapped due to technical limitations, was excluded from the analysis [21]. **C)** Mean spontaneous fMRI time course measured over the whole stimulated portion of V1. Consistent with previous studies, the signal intensity was weaker in deeper compared to more superficial depths. To exclude the potential signal instabilities at the beginning of the scan, the first 36 s were excluded from further analysis. **D)** The spontaneous fMRI time course for one randomly selected vertex. Compared to the averaged signal, data from the individual vertices across cortical depths were less correlated to each other.

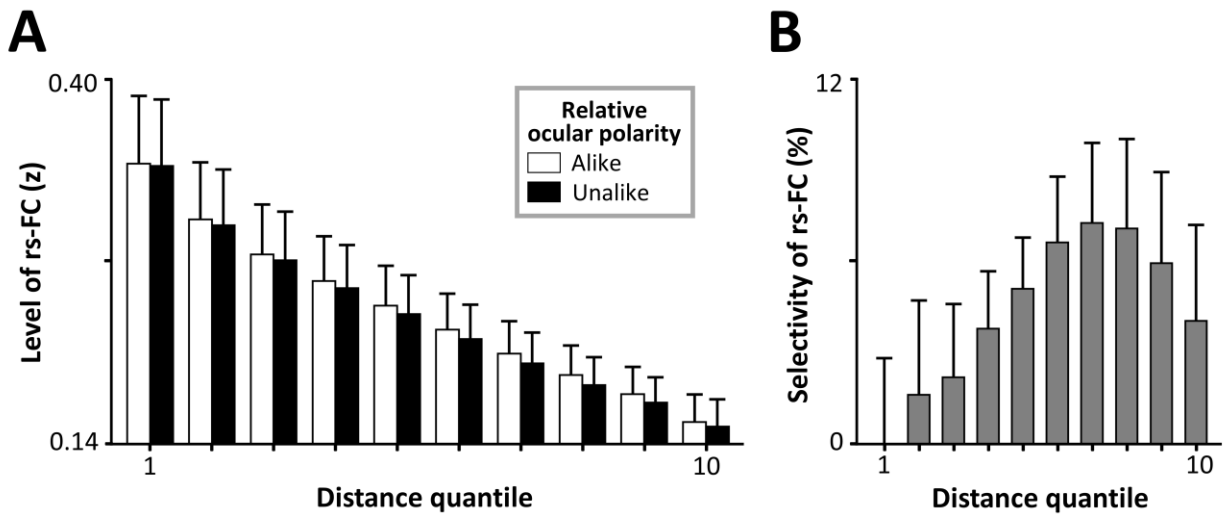

Figure 2. The rs-FC between vertex pairs and its selectivity in favor of the pair with alike ocular polarity as a function of distance. **A)** Mean rs-FC levels across subjects are displayed as *z*-values for vertex pairs with alike (white bars) and unalike (black bars) ocular polarity for 10 distance quantiles (with 1 being the closest but excluding vertices closer together than 3mm due to fMRI PSF (see Methods) and 10 being the farthest distance (Figure S1)). Rs-FC decreased with increasing distance. **B)** Selectivity of rs-FC, measured as the alike rs-FC minus the unalike rs-FC and normalized for overall rs-FC level, is depicted for each distance quantile in percentage. In both panels, error bars represent the standard error of the mean.

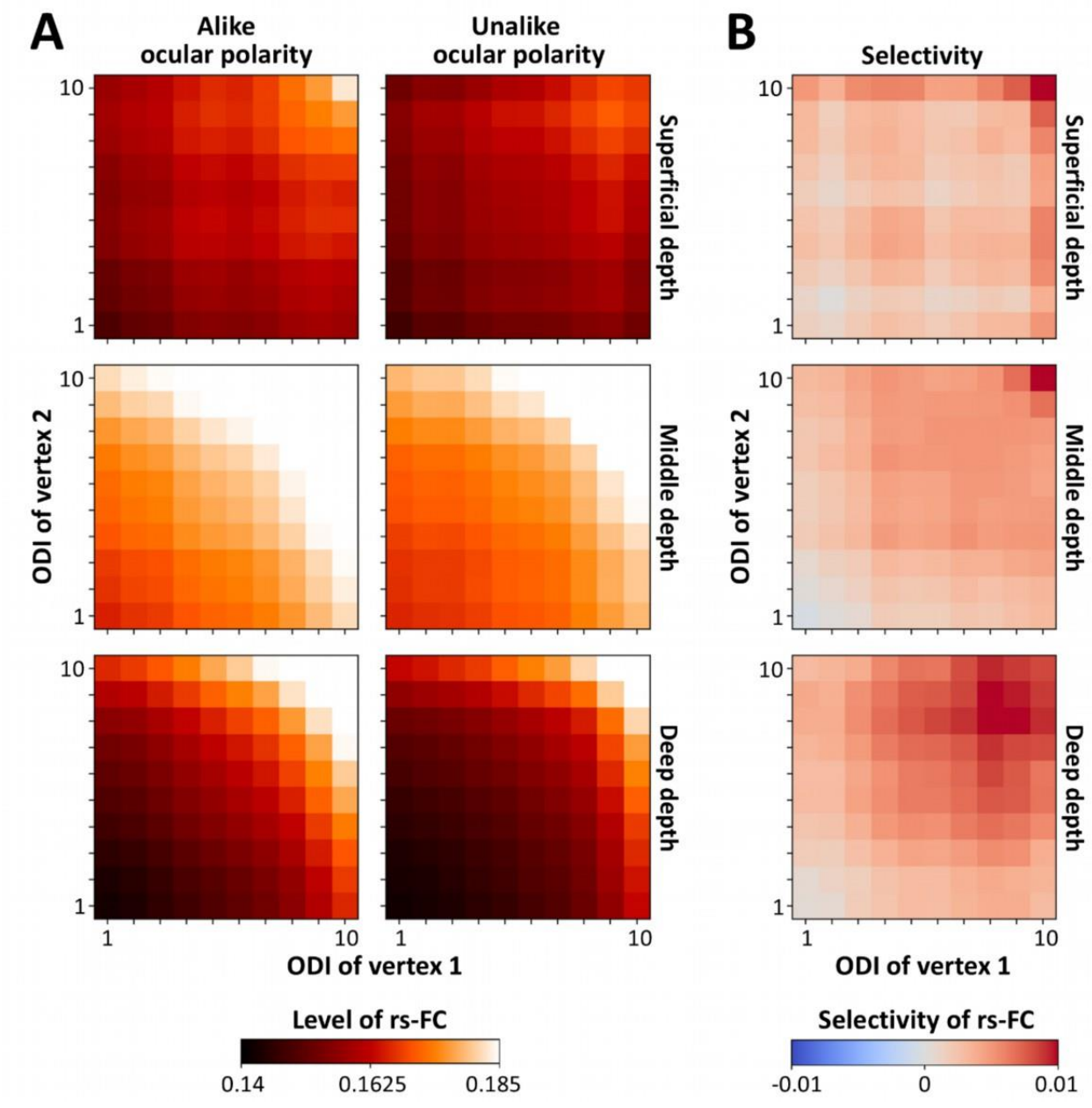

Figure 3. The measured rs-FC between V1 vertex pairs and its selectivity as functions of cortical depth and ODI averaged over all participants. **A)** The level of rs-FC between vertex pairs with alike (left) and unalike (right) ocular polarity measured across superficial (top), middle (middle), and deep (bottom) cortical depths. Each correlation matrix shows the mean rs-FC measured as *z*-values. In each matrix, *x*- and *y*-axes represent the ODIs of vertex pairs categorized in quantiles 1 to 10 representing low to high ODI beta values (Figure S3). The measured rs-FC is generally higher at middle cortical depth and increases with ODI. **B)** Selectivity is defined as the difference between rs-FC of vertex pairs (alike minus unalike ocular polarity) without any normalization. The selectivity was generally higher, favoring pairs

with alike ocular polarity and increased for vertex pairs with higher ODI.

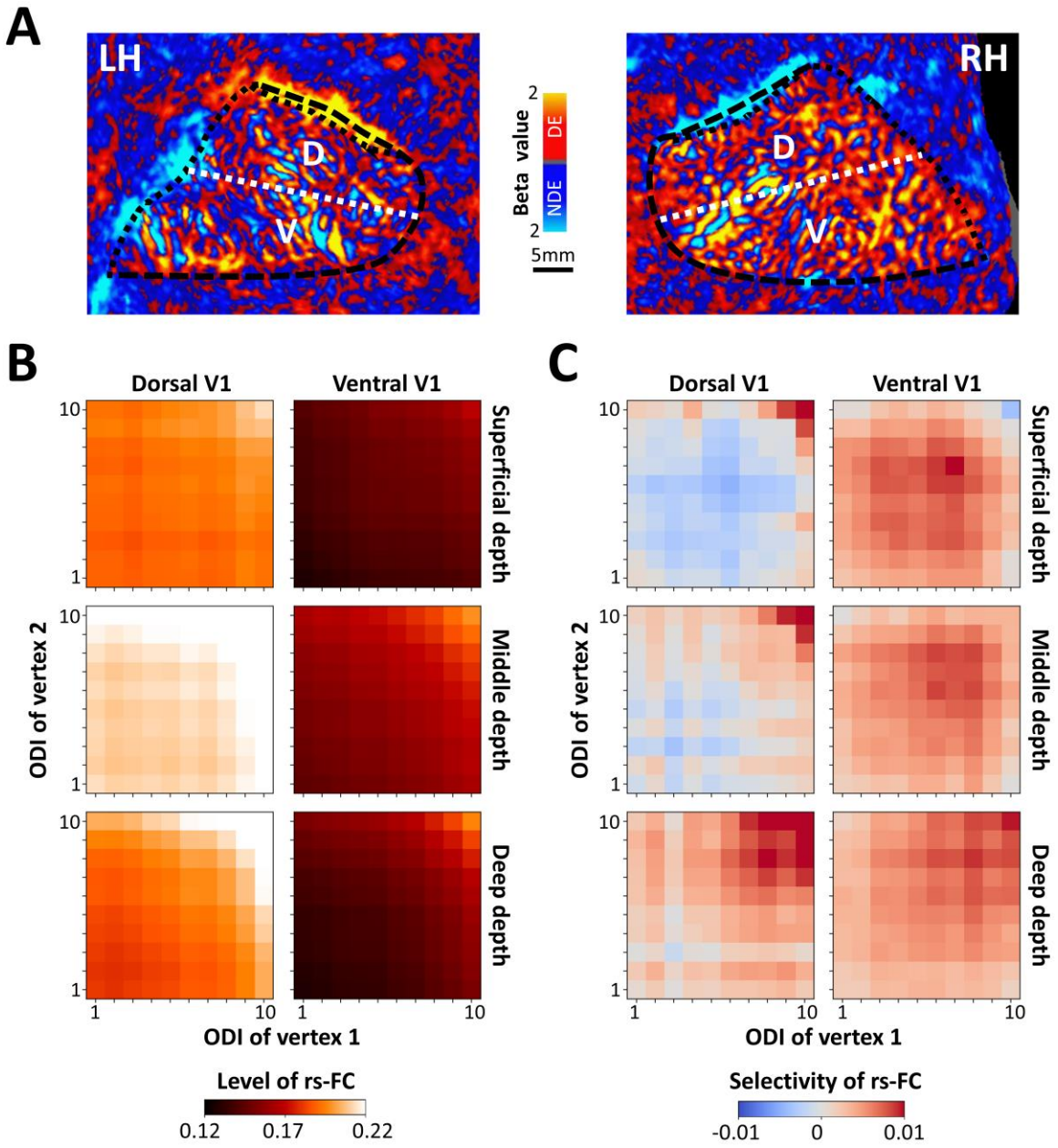

Figure 4. Comparison of rs-FC and selectivity between ventral (V) and dorsal (D) V1 averaged across all participants. **A)** Location of dorsal and ventral V1 subregions, overlaid on the ODC map in the left and right hemispheres from one participant (other than the one shown in Figure 1). The stimulated part of V1 (dashed and dotted black lines) was divided into two equally sized areas along the calcarine sulcus (dashed white line). **B)** The measured rs-FC between (all) vertex pairs in dorsal (left) and ventral (right) V1 subregions irrespective of relative ocular polarity. The rs-FC level was on average higher in dorsal compared to ventral V1 subregion. **C)** The selectivity of rs-FC across the two subregions. In dorsal V1 subregion, the selectivity was more confined to sites with high ODI whereas in the ventral V1 subregion, the selectivity was more uniformly distributed across ODI. The other details are the same as in Figure 3.

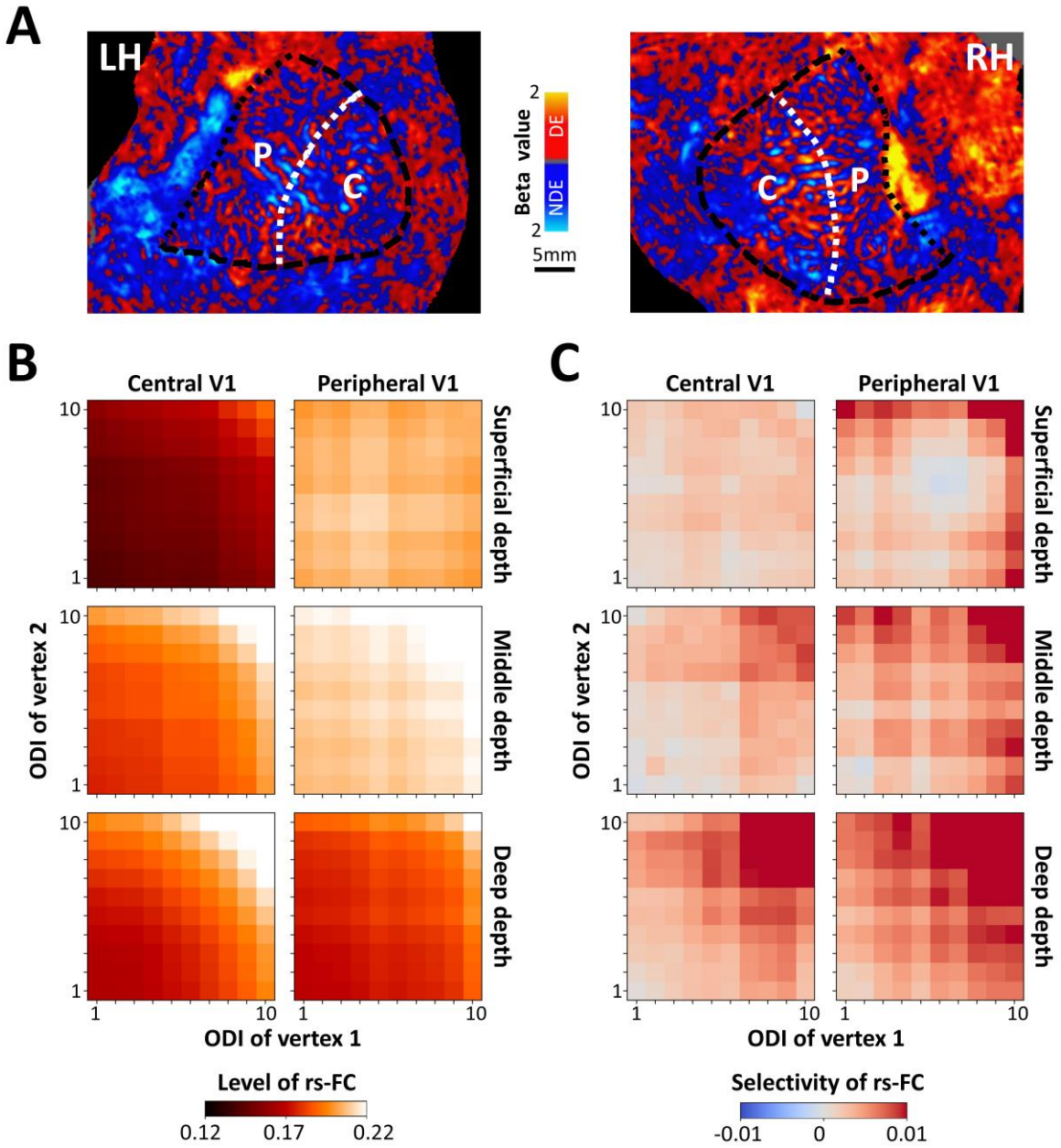

Figure 5. Comparison of rs-FC and selectivity between central (C) and peripheral (P) V1 averaged across all participants. **A)** Central (radius<4º) and peripheral V1 subregions are shown relative to the ODC map in one participant (other than the one shown in Figures 1 and 4). **B)** The level of rs-FC was on average higher in peripheral V1 compared to central V1, which was more apparent in superficial and middle depths. **C)** Likewise, the selectivity of rs-FC was higher in the peripheral compared to the central V1 subregion in superficial and middle cortical depths. The other details are similar to Figure 4.

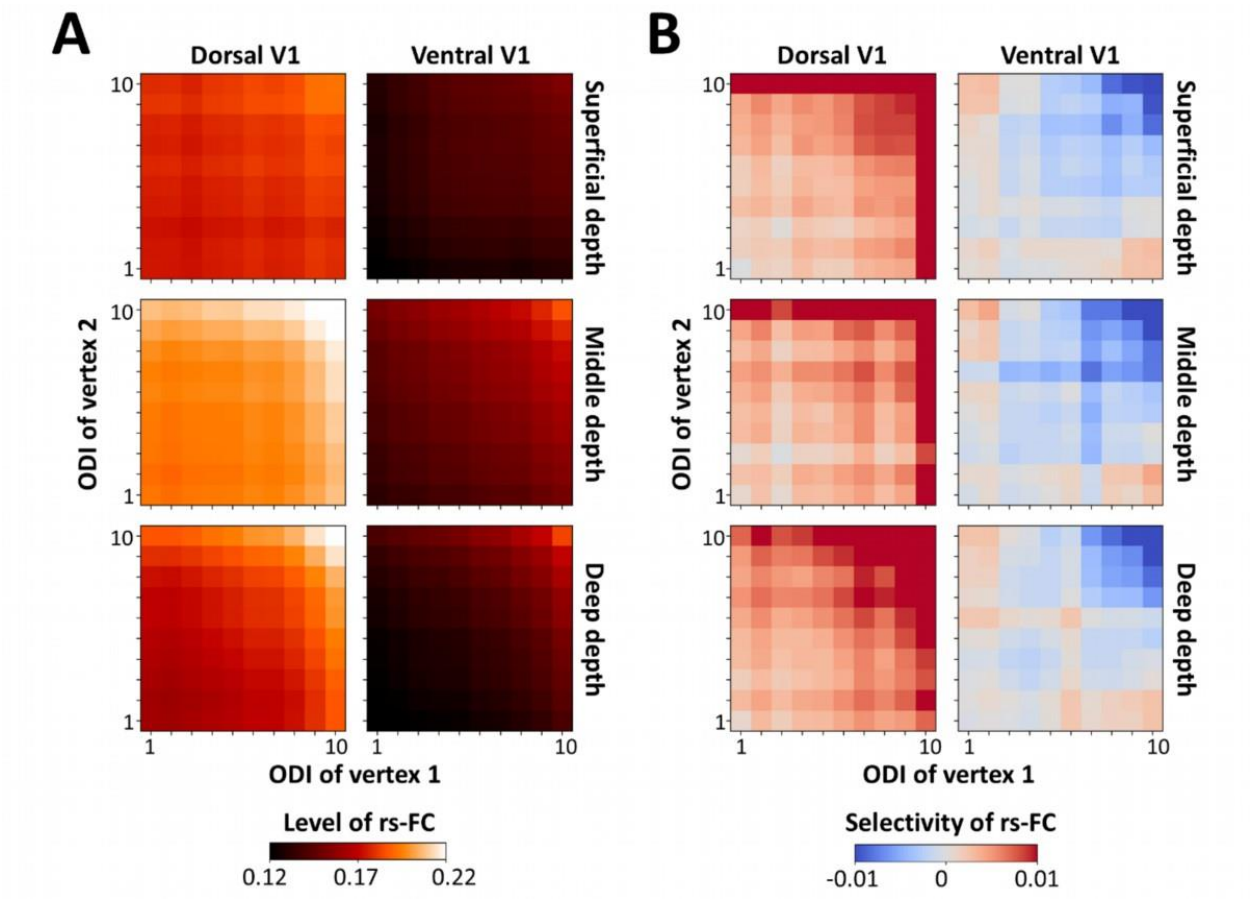

Figure 6. Interhemispheric rs-FC and its selectivity for vertex pairs located within dorsal and ventral V1 subregions averaged across all participants. **A)** Similar to the intrahemispheric rs-FC, the interhemispheric rs-FC was higher in the dorsal compared to ventral V1 subregion. The effects of cortical depth and ODI that were observed for intrahemispheric rs-FC are preserved for interhemispheric rs-FC. **B)** In the dorsal V1 subregion, the selectivity of rs-FC was stronger and in favor of pairs with alike ocular polarity. Whereas in the ventral V1 subregions, the selectivity appeared to be weaker and reversed (i.e. in favor of vertex pairs with unalike ocular polarity). The other details are similar to Figure 4.

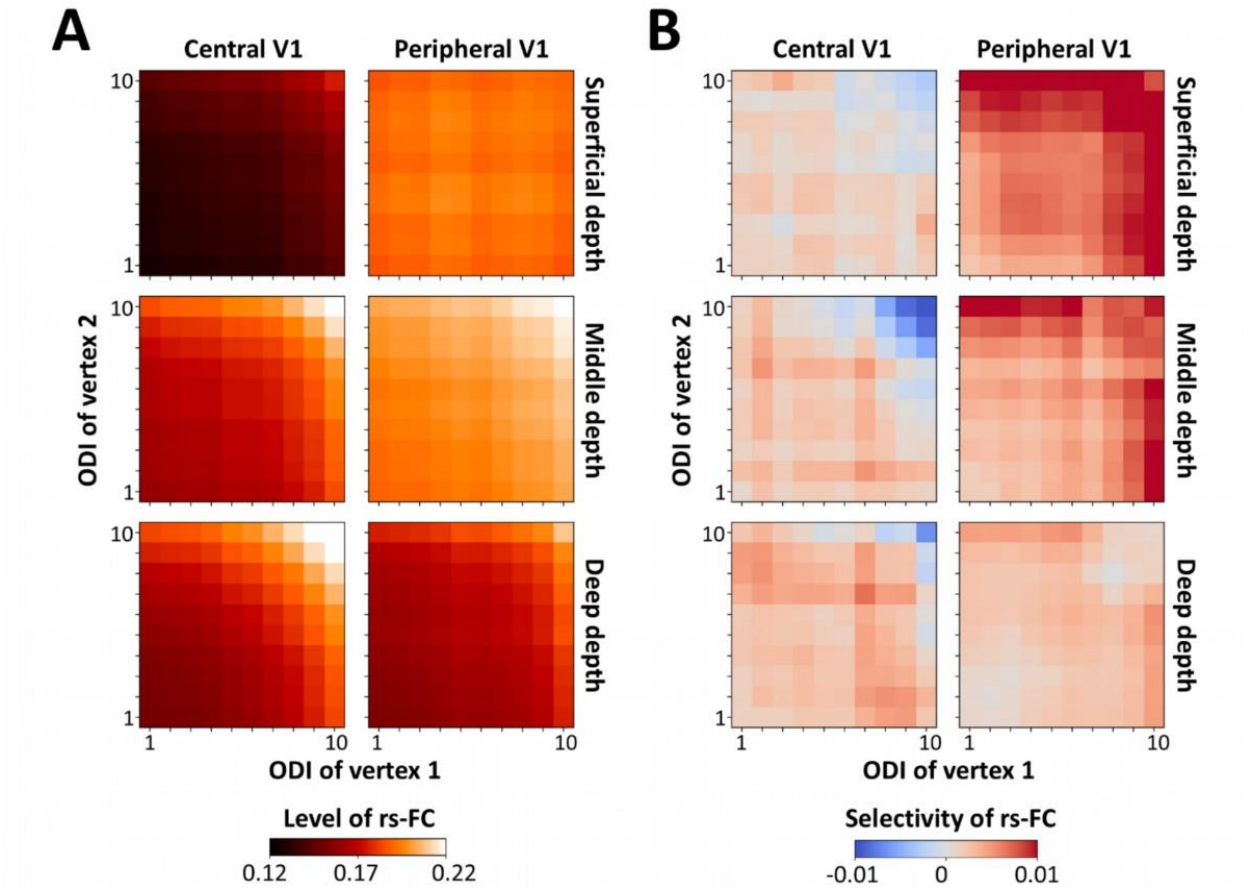

Figure 7. Interhemispheric rs-FC and its selectivity for vertex pairs located within central and peripheral V1 subregions averaged across all participants. **A)** The level of interhemispheric rs-FC was, on average, higher in the peripheral compared to the central V1 subregion. Here again, this phenomenon resembles what we detected for the intrahemispheric rs-FC (Figure 5). **B)** The selectivity of rs-FC was higher in peripheral compared to central V1 subregions mainly in superficial and middle cortical depths. The other details are similar to Figure 4.

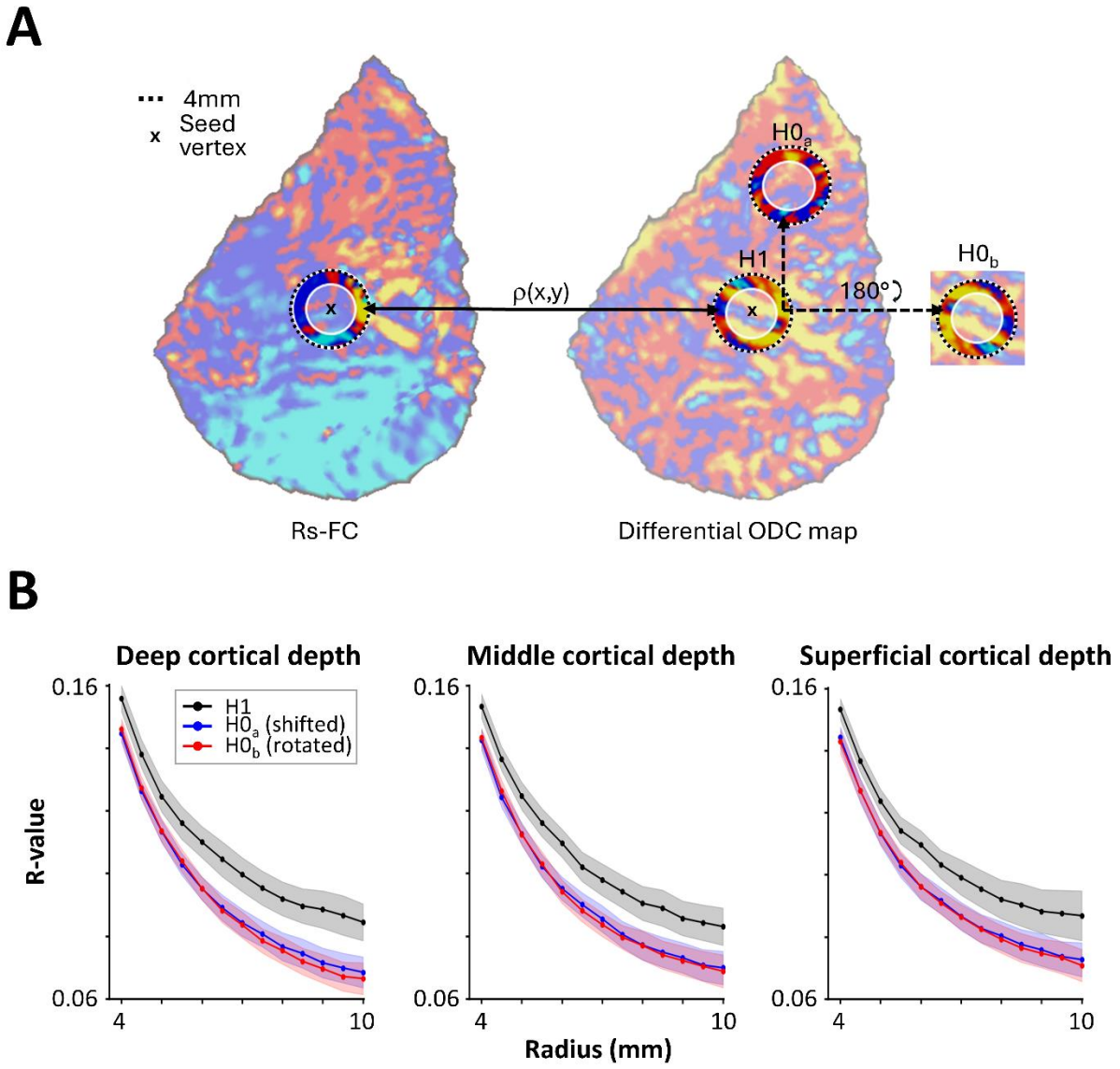

Figure 8. Correlation of rs-FC with the differential ODC map. **A)** Schematic figure showing a map of rs-FC obtained by correlating the time-series of one seed vertex (x) with all other vertices (left) and the corresponding differential ODC map of that representative subject and hemisphere (right). Ring-shaped regions of the rs-FC map with varying outer radii and fixed inner radius of 3mm (white shaded inner circle, to exclude vertex pairs within the fMRI PSF) were correlated with the ODC differential map at either the ring at the same location (H1) or a shifted location ($H0_a$) or the same location but rotated by 180° ($H0_b$). **B)** Resulting *r*-values (*y*-axis) averaged across participants are plotted as a function of the ring radius (*x*-axis) for the three different comparisons using rs-FC sampled at the three different cortical depths. The shaded areas correspond to the respective standard error of the mean. For all cortical depths and radii, *r*-values of the H1 were significantly higher than for the two null hypotheses (H0) indicating that the correlation is not only influenced by the overall topography of ODC patterns.